American Journal of Applied Scientific Research
2025, Vol. 11, No. 4, pp. 193-202
https://doi.org/10.11648/j.ajasr.20251104.12

Research Article

Comparative Study on Graphene Aerogels Prepared by Different Methods and Their Adsorption for Organic Solvents

Zian Yang, Qingwang Liu, Zhongliang Hu*

College of Materials Science and Engineering, Hunan University of Technology, Zhuzhou, China

Abstract

The atmospheric drying and freezing drying were utilized to prepare graphene aerogels (GAs), and the effect of the different drying methods and the key parameters on their structures and properties were comparatively investigated. Three kinds of GAs were synthesized using different reduction and drying ways. GA1 was prepared by subtly regulating the structure of the hydrogel and using an atmospheric drying, while GA2 and GA3 were prepared using a common reduction and freezing drying method. The results shows that GA1 possesses a uniform pore structure constituted by lamellar interconnected graphene oxide (GO) sheets with little of stacking texture, and it is super elastic and can restore to its original shape even after 90% strain. GA1 also has a high adsorption capacity ranging from 90.47-167.24 times of its own mass and a rapid adsorption efficiency toward organic solvents and in addition it possess excellent recyclability. The comparative study indicated that GA1 far surpasses GA2 and GA3 in performance and structure. The study on the formation mechanisms revealed that the subtly regulated structure of the hydrogel is of key importance to the atmospheric drying, and the capillary force up on this drying can be utilized to adjust its pore structure. It is the firstly attempted to investigate the roles of reduction and drying methods upon preparing GAs, and the results will be of great importance to guide the synthesis, design, structure optimization and performance improvement of GAs.

Keywords

Graphene Aerogel, Chemical Reduction, Hydrothermal Reduction, Atmospheric Drying, Pore Structure

1. Introduction

Graphene is of 2D honeycomb structure formed by carbon monolayers, and it has many outstanding properties, so graphene has become a research hotspot in materials and their related subjects since its discovery in 2004 [1-5]. Due to its low synthesis cost, Graphene Oxide (GO) has been thought as a good precursor to prepare graphene materials. However, graphene has a strong tendency of aggregation to form graphite due to the robust π-π stacking and van der Waals force between its sheets, thus greatly deteriorating its performance [6, 7]. To prevent it from stacking, the researchers have adopted the means of composing graphene with nanomaterials [8-10], but these ways could not thoroughly resolve the agglomeration of graphene. Until 2009, 3D graphene aerogels (GAs) had been firstly reported by Wang and Ellsworth [11], and their special 3D structure can well restrain the accumulation of graphene sheets. Moreover, the prepared

*Corresponding author: david10103@sina.com (Zhongliang Hu)

Received: 16 September 2025; **Accepted:** 9 October 2025; **Published:** 31 October 2025

GAs show an excellent conductivity and a high surface area, far surpassing the traditional carbon aerogel in performance.

GAs, macrostructural monoliths, utilize graphene sheets as building blocks to construct 3D networks, in which the graphene sheets crosslink and support each other, greatly lowing the π-π and van der Waals force between graphene sheets. Therefore, GAs can fully maintain the specific properties of graphene. Meanwhile, GAs possess ultralow apparent density, large specific surface area, excellent compressibility, high conductivity and abundant hierarchical pore structure [12-14]. As a consequent, GAs have attracted more and more concern in the academic and industrial community [15-17]. At present many methods have been invented to synthesize GAs, including chemical vapor deposition, liquid phase assembly (LPA), 3D printing, and so forth. Among them, the LPA method has been most largely investigated due to its facile preparation and cost-effectiveness [18, 19]. For example, Zhao et al [12] used GO and pyrrole as precursors to obtain a versatile, N-doped, ultralight 3D GAs by hydrothermal reaction, lyophilization and subsequent heat treatment, and the resulting GAs show excellent adsorption capacities for organic liquids. They also have a high specific capacitance of 484 F/g, and exhibit a high electrocatalytic activity toward ORR reaction. For better improve the performance, recently lignin, cellulose and bio-mass materials have been employed to adjust the structure of GAs and these modified GAs have largely improved their mechanical strength and exhibit promising application in environmental remediation such as oil/water separation and adsorption to microplastics, dyes, oil and heavy metal ions [20-24].

The above LPA preparation researches undoubtedly have contributed much to the development of GA subject, but it generally adopts freezing drying or supercritical gas drying to remove the solvents. The drying method is time-consuming and energy-consuming, and it needs expensive equipment. More recently, Yao et al [25] took advantage of the reinforcement of a few carbon nanotubes, an atmospheric drying method had been developed to get rid of the solvents in graphene hydrogels, and the resultant GAs own excellent electrical and mechanical properties, therefore they are very suitable to be used as piezoresistive sensors. Zhao et al [26] also utilized the atmospheric drying to prepare GAs, and the thus obtained GAs are highly compressible and super-elastic with high adsorption capacities for organics. Obviously, the atmospheric drying means could greatly decrease the preparation cost, and in consequence it would significantly accelerate the commercial applications of GAs. Unfortunately, the previous studies mainly focused on the investigations of the preparation and performance of GAs, and few researches explored the effect of the atmosphere drying on the structure and performance of GAs. For example, in what conditions could freeze drying be replaced by atmosphere drying, not resulting in the structure collapse of GAs? Could the drying way affect the structure of GAs and how it influences their structure? It will be of key importance to explore these issues for the further development of this subject.

In this paper, several kinds of GAs were synthesized by hydrothermal and chemical reduction, and subsequent freeze drying or atmospheric drying was utilized to get rid of the solvents. The thus obtained GAs were comparatively studied to investigate the effect of reduction and drying methods on the structures and properties of GAs. For property examination, several organic solvents were chosen as adsorbates to inspect the adsorption and recyclability performances of GAs. To the best of our knowledge, it is firstly attempted to systematically investigate the roles of the reduction of GO and drying of hydrogels upon preparing GAs, and the results will be of great importance to guide the synthesis, design, structure optimization and performance improvement of GAs.

2. Experimental

2.1. Materials and Chemicals

GO power prepared by Hummers' method [27] was bought from Jiangsu Xianfeng nanomaterials Co. Ltd., and its CAS No. is 7440-44-0. The lateral size of GO sheets ranged from 0.5 to 5 μm. L-ascorbic acid, ethanol, cyclohexane, dimethyl sulfoxide and carbon tetrachloride were purchased from Sinopharm Chemical Reagent Co. Ltd. China. All chemicals are of analytical regents and were used as received.

2.2. Synthesis of GAs

Three kinds of GAs were successfully prepared based on their optimized parameters and the detailed synthesis processes were described below.

16 mg GO was added into a beaker containing 8 ml distilled water and the GO dispersed solution had been ultrasonicated for 30 min to form a uniform solution. Then, 32 mg L-ascorbic acid was added into the GO solution, and the mixture solution was stirred for 5 min and then transferred into a 10 ml Teflon-lined autoclave. After chemical reaction at 80 ℃ for 45 min, the resultant hydrogel was frozen at -18 ℃, then thawed for 2 h. After being frozen/thawed for 3 circles, the sample was treated again at 80 ℃ for 6 h, washed with ethanol until ethanol has no yellow color, and then immersed into ethanol for 6 h. Finally, the thus obtained sample had been dried in an oven at 50 ℃ for 24 h at an atmospheric pressure, and the GA is denoted as GA1.

The hydrogel of the second sample was prepared based on the same procedures as GA1 except that 16 mg L-ascorbic acid instead of 32 mg dosage was used and the chemical reaction time prolonged from 45 min to 60 min. After formation of the hydrogel, it was put into 20% ethanol solution for 6 h to get rid of the impurities, and freeze-dried at -50 ℃ for 24 h, resulting in the GA2 sample.

For synthesis of the third GA sample, 8 ml GO solution (2 mg/mL) was prepared by the same steps as GA1. Whereafter, the GO solution was sealed in a 10 ml Teflon-lined autoclave and reduced hydrothermally at 180 ℃ for 60 min to obtain a

hydrogel. The hydrogel was soaked in 20% ethanol solution for 6 h to remove the impurities, and freeze-dried at -50 ℃ for 24 h. The resultant GA is expressed as GA3.

2.3. Characterization

X-ray diffraction (XRD) patterns were documented on Bruker D8 Advanced Diffractometer using Cu-Kα radiation (λ = 0.154 nm) in the 2θ range of 5-90 °. The morphologies of the GA samples were observed using a field-emission scanning electron microscope (SEM) (Sigma 300, ZEISS, Germany). The Fourier-transform infrared (FTIR) spectra of the sample were collected by FTIR spectrometer (Thermo Scientific Nicolet iS20, US) and the data were recorded in the wavenumber range of 400-4000 cm-1. N_2 adsorption tests were conducted at 77 K using BET specific surface area (SSA) analyzer (ASAP 2460, US). The SSAs of the samples were also measured by methylene blue adsorption (MB) method using MB as a molecule probe [28].

2.4. Adsorption Experiment

The adsorption capacity of the sample was evaluated using ethanol, cyclohexane, dimethyl sulfoxide and carbon tetrachloride as absorbates. The aerogel was weighed and then immersed in the solvents until saturation was reached. Afterwards, the sample was quickly taken out with a tweezer and the excess solvent on its surface was removed to get the adsorption mass. The adsorption capacity was calculated based on the following equation [29]:

$$Q = (W - W_0)/W_0 \quad (1)$$

where Q represents the adsorption capacity of the GA sample, and W_0 and W are the weighs of the sample before and after adsorption.

3. Results and Discussion

3.1. Aerogel Morphology and Elasticity Analyses

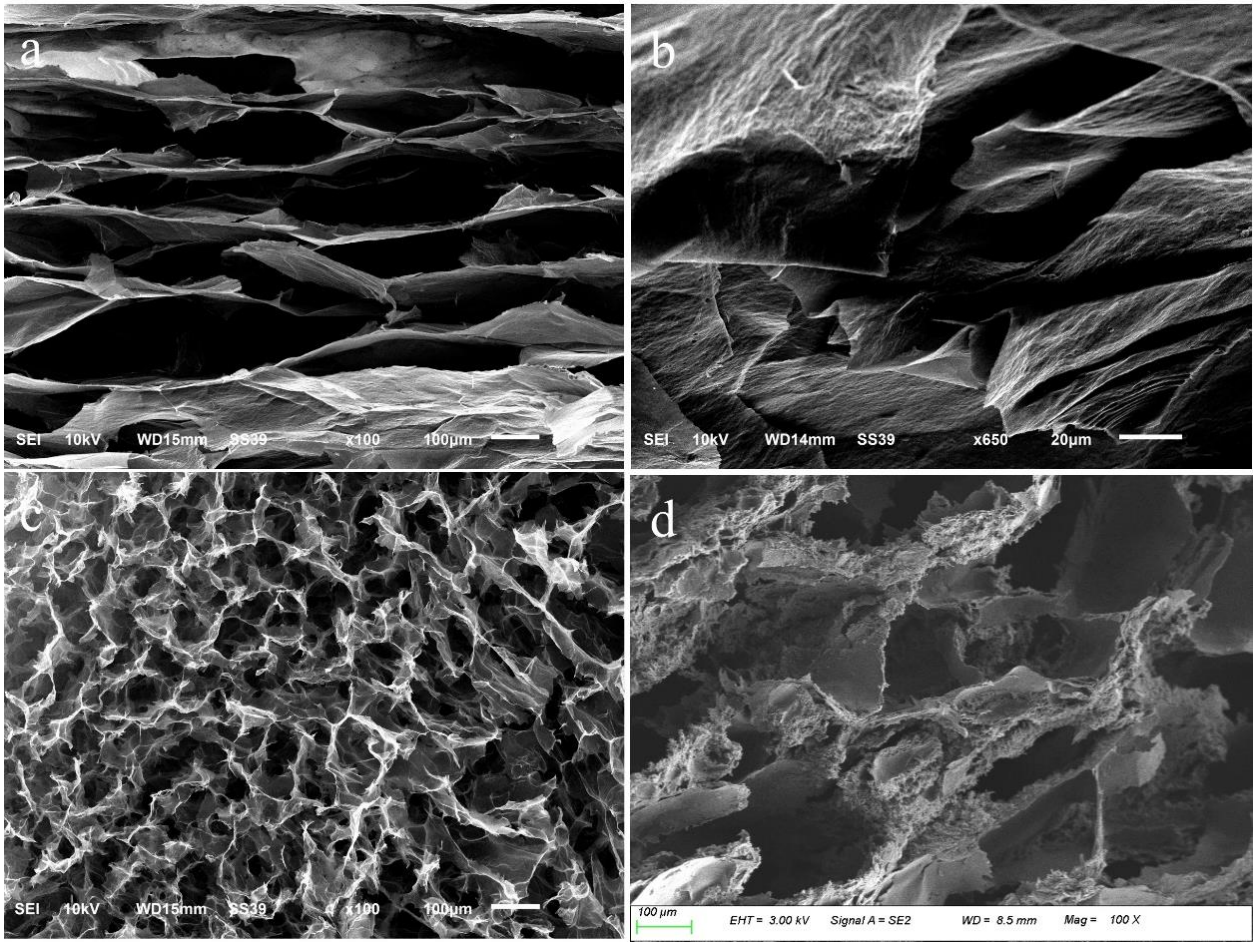

Figure 1. *SEM images of the GA samples: a-b GA1, c GA2, and d GA3.*

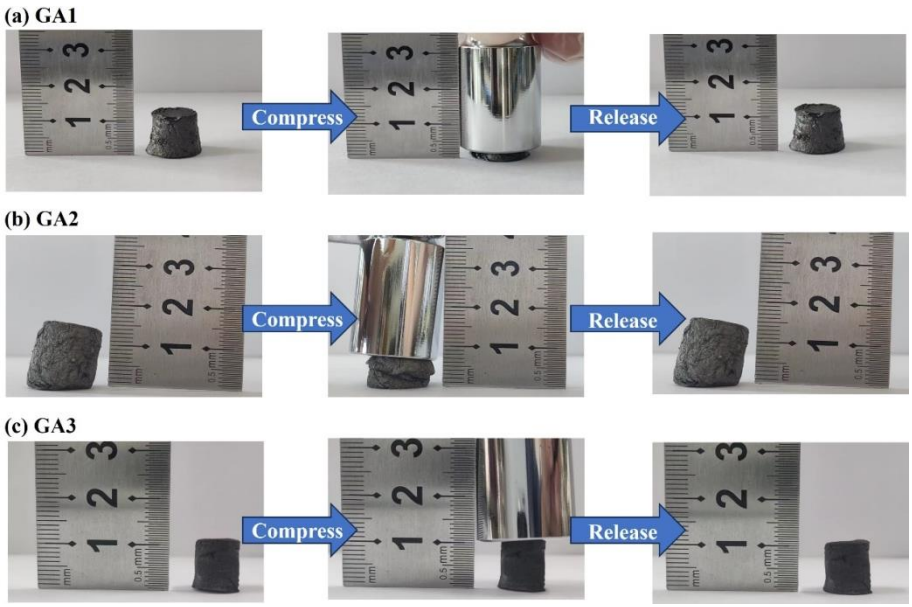

Figure 2. *The photographs of GAs under different strain levels: a GA1, b GA2, and c GA3.*

The morphologies of the GAs are displayed in Figure 1. Obviously, they present distinct appearances, in contrast to each other. From Figure 1(a) and (b), it can be clearly observed that the graphene sheets in GA1 are well separated and they are interconnected and supported by each other, and they are arranged in lamellar structure, forming uniformly distributed pores. The more magnified SEM image (Figure 1(b)) shows that the GO sheets are very thin, inferring that no evident stacking of graphene sheets happened. In GA2, the graphene sheets are interweaved each other to form open pores, which are formed by the induction of ice crystal. and in some place accumulation of graphene could be faintly observed, indicative of a little stacking of GO sheets (Figure 1(c)). By contrast, GA3 exhibits remarkable aggregations of graphene sheets, and the stacking of graphene sheets is so severe that it is hard to distinguish the GO sheets in this sample. The stacked GO sheets are linked to constitute the wall of pores.

The micromorphology and microstructure of the samples would affect their elasticity property. Figure 2 displays the compression/release processes of the GA samples. It can be seen that GA1 can restore its original height ever after 90% strain, indicating that it is super elastic. GA2 can resist 60% strain without visible plastic deformation. However, GA3 is brittle and its fragility can be attributed to the significant stacking of GO sheets [20], so that it can only endure 10% strain.

3.2. Aerogel Structural Characterizations

The XRD patterns of the GO and GA samples are presented in Figure 3. From the figure, it can be seen that GO has a sharp peak at ~2θ=10.4°, which is attributed to its (001) lattice plane, and GAs present a broad peak at ~2θ=25°, corresponding to the (002) peak of graphite [6]. Compared with the other aerogel samples, GA3 shows a much stronger (002) peak and it can be explained that GO has been partly reduced and the reduced GO sheets has considerably stacked to form graphite flakes, resulting a sharp graphite (002) peak. In contrast to GA3, the GA1 and GA2 samples exhibit weak (002) peak, suggesting that most graphene sheets are not aggregated and they are arranged in an irregular structure, which is good agreement with the results of SEM images.

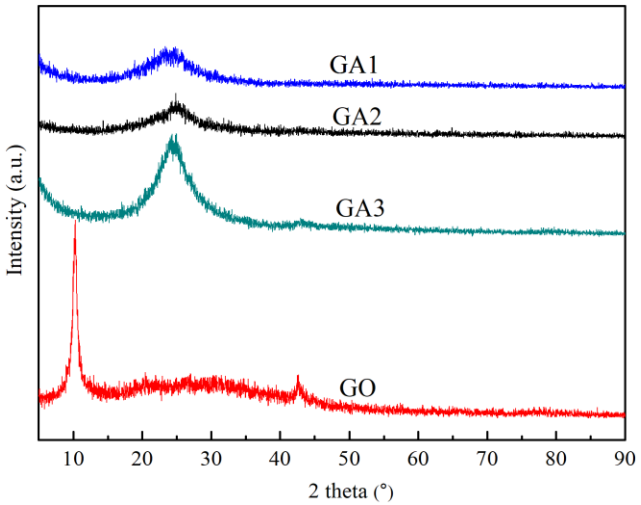

Figure 3. *XRD patterns of the GA samples.*

The evolution of chemical groups in GAs was investigated by FTIR spectroscopy, and the results are shown in Figure 4. The rich functional groups of GO are distinctly reflected in its FTIR spectra. The peaks at 3620 and 1740 cm^{-1} are characteristic ones of GO and they are attributed to the O-H and C=O stretching vibrations from carboxyl groups, respectively. The broad peak at 3320-3460 and 1610 cm^{-1} are ascribed to the O-H stretching

vibration and bending motion, respectively [3, 5]. The peak at 1245 cm^{-1} is assigned to the C-OH bending motion and the peak at 1030 cm^{-1} is due to C-O-C of epoxy. After hydrothermal/chemical reduction, the peaks at 3620, 3320-3460 and 1030 cm^{-1} almost disappear, and the peaks at 1740, 1610 and 1245 cm^{-1} become much weaker, indicating that some functional groups have been removed and GO has been partly reduced. From the evolution of the peaks, it can be seen that GA1 has been most thoroughly reduced, GA2 possesses an inferior reduction degree, and GA3 has the lowest reduction degree.

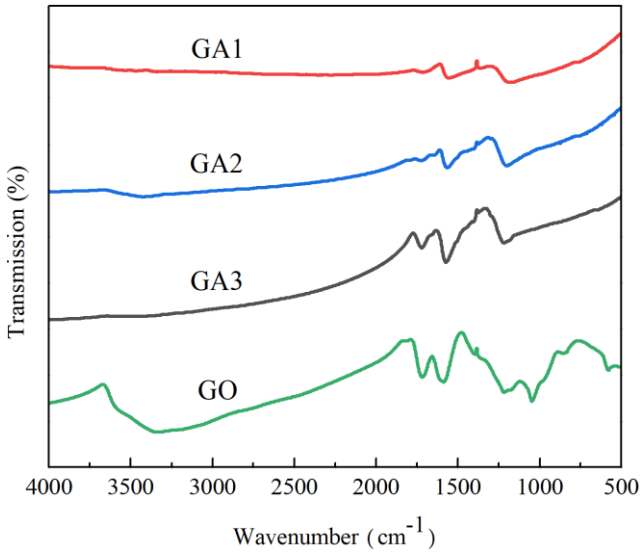

Figure 4. *FTIR spectra of GO and the GA samples.*

To further explore the structure of GAs, N_2 adsorption-desorption tests were carried out on the GAs samples and the data are shown in Figure 5. GA1 displays a typical IV-type curve with a H_2 hysteresis loop, inferring that it contains some mesopores. Both of GA2 and GA3 have inapparent hysteresis loops, suggesting that they possess little mesopores. All aerogel samples present low adsorption to N_2 at low pressure stage, but the adsorption amounts increase sharply when relative pressure approaches 1.0, manifesting that the samples have a neglectable micropores and a great number of macropores. Because N_2 adsorption test is mainly suitable to measure micropores and mesopores [30], MB was also utilized as adsorbates to further survey the specific surface area (SSA). Table 1 listed the apparent densities and their SSAs of the GA samples measured by N_2 and MB adsorption methods. The three samples used the same GO concentration to prepare the GAs, but GA3 has an apparent density of 13.05 mg/cm^3, much larger than those for GA1 (7.78 mg/cm^3) and GA2 (7.61 mg/cm^3) and it is caused by its severe GO stacking structure, inevitably enhancing its density. Compared with other carbon materials, GAs own an ultralow density, resulting in their ultrahigh porosity, so they have much larger pore diameters than traditional carbon materials, which lay beyond the range accessible to N_2 adsorption [30]. The great data differences between N_2 and MB adsorption tests further demonstrate that the GA samples are mainly composed of macropores, which is in good agreement with SEM results. Among the three kinds of GAs, GA1 had the highest MB SSA, reaching 963.86 m^2/g. This figure is equal to 36.6% of the theorical SSA of graphene, which is 57.1% greater than GA2's and 166% higher than GA3's. The large SSA of GA1 can be attributed to its dispersive structure of GO sheets, in which the ultrathin graphene sheets are interconnected and supported each other, effectively preventing them from stacking into graphite agglomerations. In contract, GA3 has a low MB SSA (362.48), and this can be attributed to its significant stacking of graphene, lowing the accessible area for MB molecules.

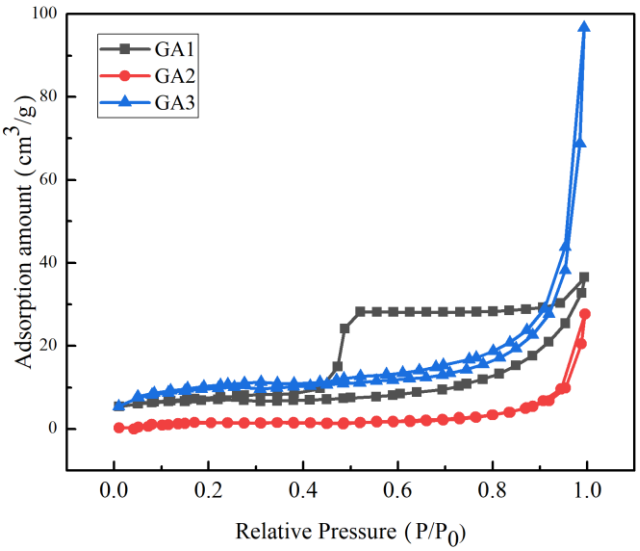

Figure 5. *N_2 adsorption isotherms for GA1, GA2 and GA3.*

Table 1. *The apparent density, and their BET and MB SSAs of the GA samples.*

Sample	Density (g/m^3)	BET SSA (m^2/g)	MB SSA (m^2/g)
GA1	7.78	25.57	963.86
GA2	7.61	16.64	613.59
GA3	13.05	35.28	362.48

3.3. Adsorption Capacity and Recyclability

The structure analyses demonstrated that the GA samples are of high porosities which are beneficial to adsorption toward organic compound and oils [31, 32]. As a result, four pure organic solvents (ethanol, cyclohexane, dimethyl sulfoxide and carbon tetrachloride) were used as adsorbates to measure the capacities of the GAs samples, and the results were presented in Table 2. Obviously, GA1 possesses a highest adsorption toward the tested solvents while GA3 displays a lowest capacity. The adsorption capacities of GA1 range from 90.47 to 167.24 g/g, which are also greater than other reported GAs [24, 26, 33]. It is worth noting that the capacities are approximately proportional to the solvent density, inferring that the adsorption is a volume filling behavior [34]. Nevertheless, the samples display different volume filling degrees (VFD) of solvents, which are 86.3%, 76.3% and 66.0%, respectively, corresponding to GA1, GA2 and GAs. The high VFD of GA1 means that its pores are mostly connected with open channels, while GA3 has only 66% VFD, indicating that some pores cannot be reached by solvent molecules. This can be explained that there exist graphene sheets to stack into graphite in GA3 and there are more open pores in GA1 and GA2, which is in good agreement with the results of SEM and XRD characterization.

Table 2. *Solution density and adsorption capacity for the GA samples.*

Organic species	Density (g/m^3)	GA1 (g/g)	GA2 (g/g)	GA3 (g/g)
Cyclohexane	0.778	90.47	81.93	40.66
Ethanol	0.789	89.87	82.04	39.28
Dimethyl sulfoxide	1.100	120.95	108.82	54.56
Carbon tetrachloride	1.592	167.24	148.07	75.40

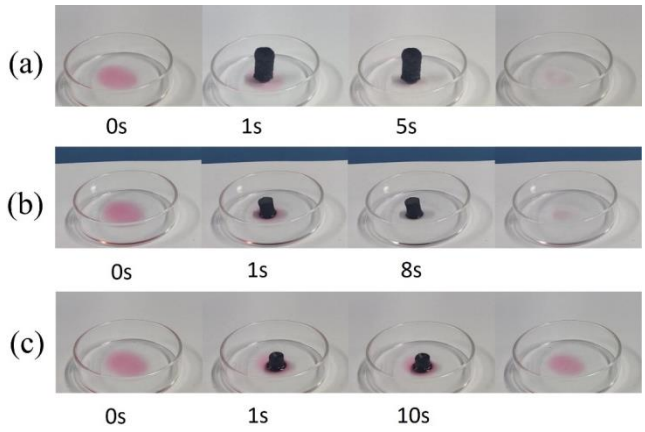

Figure 6. *The pictures of the samples adsorbing carbon tetrachloride (dyed with Sudan III) from the bottom: a GA1, b GA2, and c GA3.*

To further evaluate the adsorption efficiency, the GA samples was utilized to adsorb solvents from the bottom of the samples. As shown in Figure 6, 0.3 ml carbon tetrachloride can be completely adsorbed in 5 s by GA1 and in 8 s by GA2 while GA3 can only adsorb a little of the solvent in 10 s. Obviously, the adsorption impetus comes from the capillary force, demonstrating that GA1 has a highest adsorption efficiency and the strongest capillary force. In contrast, GA3 has the worst adsorption efficiency due to the lowest capillary force. The capillary force is highly related to the pore structure, lipophilicity and interface tension of the adsorbate [35]. For GA1, the uniform pore structure and good lipophilicity (due to a high reduction degree) are main reasons for high adsorption efficiency. But for GA1, the stacked graphene sheets cannot provide enough channels and impetuses for the adsorbate and in addition it has low reduction, resulting in a worse lipophilicity.

Reusability is of key importance for GAs' commercial applications. In this paper distillation was adopted to investigate the recyclability of the GA samples, using cyclohexane as an adsorbate. The GA samples were weighted before and after each adsorption/desorption cycle and the regenerability efficiency was calculated [36]. The adsorbed GAs were placed in an oven at 70 ℃ to remove the cyclohexane adsorbate. Absorption/desorption cycle for the GA samples was presented in Figure 7. Obviously GA1 possesses the best recyclability, even after 10 cycles of absorption/desorption, it still maintains ~89% adsorption capacity toward cyclohexane, surpassing data for other reported GAs [23, 37]. The adsorption capacities of GA2 and GA3 decrease to 82% and 74%, respectively. It had been thought that the recyclability is related to the structure of GAs, and the steady and uniform structure of GA1 results in its excellent regeneration [37].

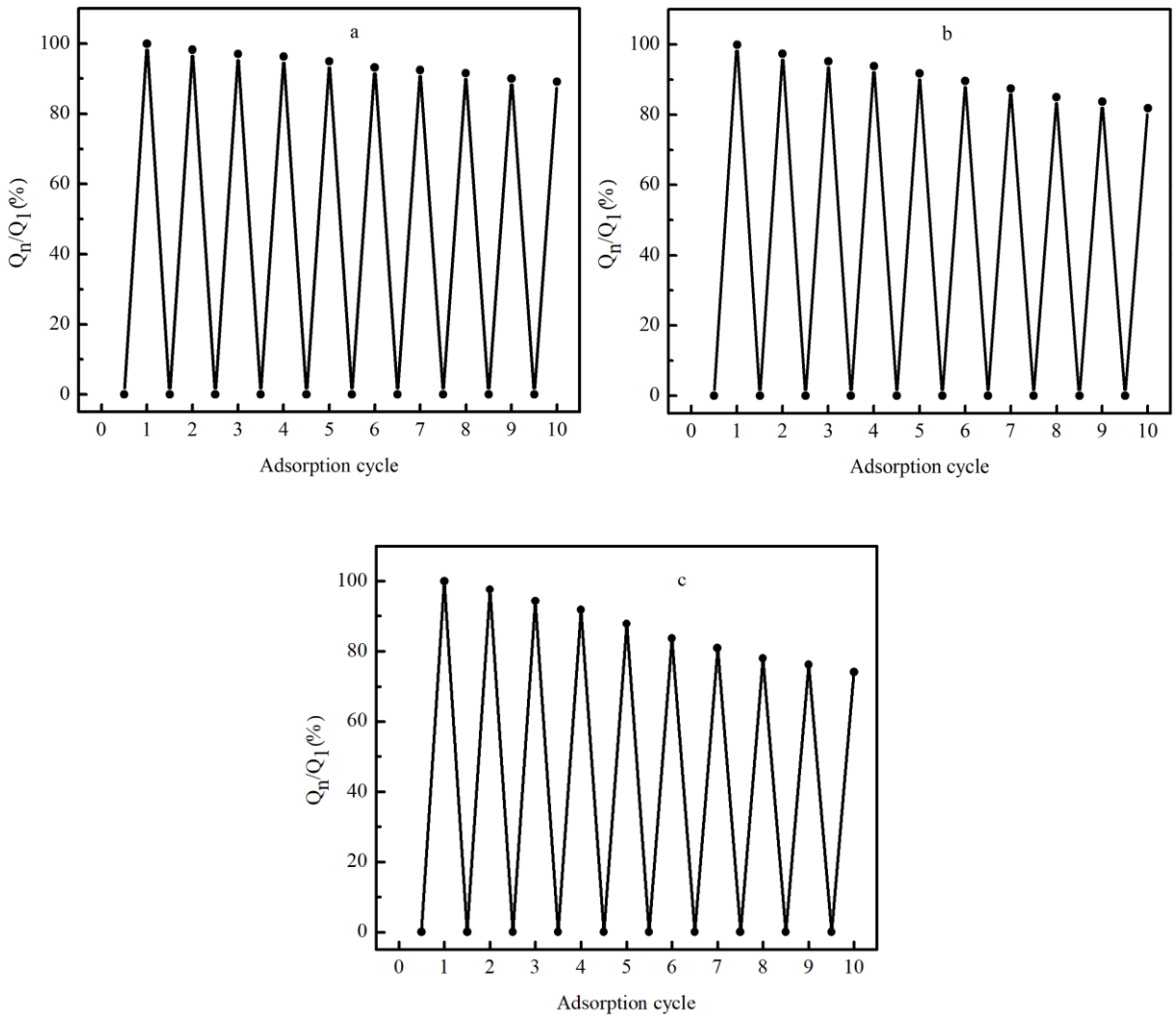

Figure 7. *Absorption/desorption cycle by distillation for: a GA1, b GA2, and c GA3.*

3.4. Analyses of Formation of GAs

The above characterizations and adsorption experiments of the GA samples proved that the GA samples have quite different structures and adsorption performances, which are highly related to their preparation methods. The formation of GA samples mainly consists of synthesis of hydrogel and drying of hydrogel. For the GA1 and GA2 samples, their hydrogels were partly reduced by chemical agents in a mild environment, they are dried by the atmospheric drying and freeze drying, respectively. For GA3, the sample was firstly hydrothermally reduced at 180 ℃, and then it adopted freeze drying to remove the solvent.

Figure 8 is the force analysis diagram of graphene hydrogel during atmospheric drying. According to Young-Laplace formula (2) [35], Pc (capillary force) is proportional to γ, cosθ and r, where γ, θ and r represent interface tension, wetting angle of the liquid and pore radius, respectively.

$$P_c = 2\gamma \cos\theta / r \quad (2)$$

The detailed preparation processes and formation mechanisms of the GA samples are depicted in Figure 9.

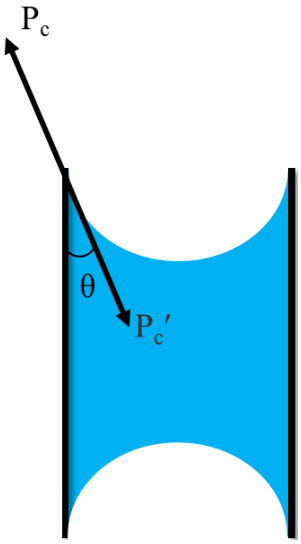

Figure 8. *The force analysis diagram of graphene hydrogel.*

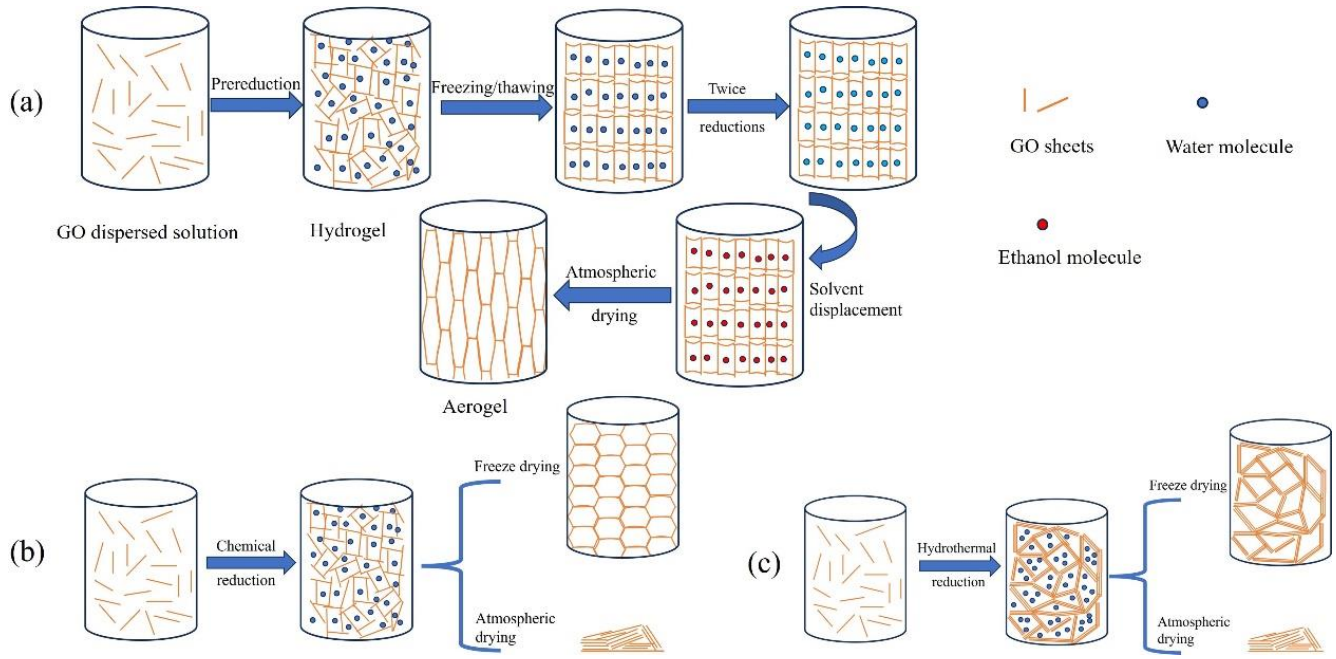

Figure 9. *The detailed preparation processes and formation mechanisms of the GA samples: a GA1, b GA2, and c GA3.*

For GA1, the GO sheets were prereduced and precipitated to form hydrogel, then freezing rearranged the GO sheets, making them directional distribution [31], and the repeated freezing and thawing further adjust the structure of the hydrogel. After solvent exchange with ethanol, the atmospheric drying was used to remove the solvent. As shown in Figure 8, Pc' is the reactive force of Pc, which acts on GO sheets, and it makes the sheets curve, resulting in a porous elastic structure constituted by directional arrangement of GO sheets.

For GA2, the reduced hydrogel was freeze dried and the thus obtained GA has an open porous structure, which comes from the ice template [38]. However, when the hydrogel was dried by the atmospheric drying, it would bring about the structural collapse of the hydrogel.

For GA3, the hydrothermal reduction was carried out at 180 ℃, the high reaction temperature can drastically agitate the partly reduced GO sheets, providing more chances for the stacking of GO sheets, and subsequent freeze drying preserve the stacking structure, endowing GA3 with obvious brittleness. Like GA2, GA3 also cannot be prepared by the atmospheric drying, otherwise its monolith structure will break down.

Among the three GA samples, only GA1 can utilize the atmospheric drying to eliminate the solvent. Based on above analyses, in this sample the capillary force is so greatly decreased that its adjusted structure can endure it. Firstly, the hydrogel is more reduced than the other samples (double reductions), making the wetting angle θ become big; secondly, ethanol displaces water, significantly lowing the interface tension γ; thirdly, the repeated freezing-thawing process adjust the structure of the hydrogel, making the GO sheets distribute more uniformly and directionally arrange at fixed volume, equally increasing the pore radium. According to Equation (2), Pc' would be largely reduced. Furthermore, Pc' can make the GO sheets more crinkle, endowing it with super elasticity.

Compared with GA1, GA2 has less reduction degree and its hydrogel has not orientation arrangements, and the precursor of GA3 has been synthesized in a violent environment, its severe stacking structure and low reduction prevent it from being dried using the atmospheric drying.

4. Conclusions

Three kinds of GAs were successfully prepared using GO as the precursor by liquid phase assembly technology. The hydrogel of GA1 was well designed, and its synthesis procedures included 3 circles of freezing-thawing, twice chemical reduction, solvent displacement, so it can endure the atmospheric drying. In GA1, the lamellar GO sheets interconnect and support each other, forming a uniform pore structure. GA2 and GA3 were roughly reduced by chemical agent and hydrothermal method. They were obtained by freeze drying, otherwise the atmospheric drying would cause the collapse of their structure. GA1 has a high SSA of 963.86 m^2/g, significantly greater than those of GA2 (613.59 m^2/g) and GA3 (362.48 m^2/g), and it has a super elasticity, which is much better than GA2 and GA3. Furthermore, GA1 has high adsorption capacity (up to 90.47-167.24 times of its own mass) to organic solvents, which is higher than GA2 and GA3, and in addition it possesses a very quick adsorption efficiency, better than GA2 and GA3. Furthermore, GA1 have an excellent recyclability. In a word, GA1 surpasses GA2 and GA3 in the structure and performance,

and its atmospheric drying method is highly efficient and cost saving. Therefore, it is very worth to systematically investigate the drying method, including the effect of reduction method, wetting angle, interface tension and capillary force on GAs. It is believed that the study will be of enlightenment to innovate the synthesis method of GAs, modify their structure and improve their performance.

Abbreviations

GAs	Graphene Aerogels
GO	Graphene Oxide
LPA	Liquid Phase Assembly
XRD	X-ray Diffraction
FTIR	Fourier-Transform Infrared
SSA	Specific Surface Area
SEM	Scanning Electron Microscope
MB	Methylene Blue

Funding

The study is financially supported by the Natural Science Foundation of Hunan Province, China (No. 2024JJ7141).

Conflicts of Interest

The authors declare no conflicts of interest.

References

[1] Novoselov KS, Geim AK, Morozov SV et al. Electric field effect in atomically thin carbon films. Science. 2004; 306(5696): 666-669. https://doi.org/10.1126/science.1102896

[2] Geim AK, Novoselov KS. The rise of graphene. Nat Mater. 2007; 6: 183-191. https://doi.org/10.1038/nmat1849

[3] Singh SB, De M. Thermally exfoliated graphene oxide for hydrogen storage. Mater. Chem. Phys. 2020; 239: 122102. https://doi.org/10.1016/j.matchemphys.2019.122102

[4] Liu J, Zhu Y, Chen X, et al. Nitrogen, sulfur and phosphorus tri-doped holey graphene oxide as a novel electrode material for application in supercapacitor. J. Alloys Compd. 2020; 815: 152328. https://doi.org/10.1016/j.jallcom.2019.152328

[5] Singh SB, Dastgheib SA. Characteristics of graphene oxide-like materials prepared from different deashed-devolatilized coal chars and comparison with graphite-based graphene oxide, with or without the ultrasonication treatment. Carbon, 2024; 228: 119331. https://doi.org/10.1016/j.carbon.2024.119331

[6] Bourlinos AB, Gournis D, Petridis D, et al. Graphite oxide: chemical reduction to graphite and surface modification with primary aliphatic amines and amino acids. Langmuir. 2003; 19(15): 6050-6055. https://doi.org/0.1021/la026525h

[7] Ma YF, Chen YS. Three-dimensional graphene networks: synthesis, properties and applications. Natl Sci Rev. 2015; 2(1): 40-53. https://doi.org/10.1093/nsr/nwu072

[8] Flores-Chaparro CE, Castilho CJ, Külaots I, et al. Pillared graphene oxide composite as an adsorbent of soluble hydrocarbons in water: pH and organic matter effects. Journal of Environmental Management. 2020; 259: 110044. https://doi.org/10.1016/j.jenvman.2019.110044

[9] Park JH, Kim KS, Wang XY et al. Highly durable graphene-encapsulated platinum-based electrocatalyst for oxygen reduction reactions synthesized by solution plasma process. J Power Sources. 2023; 580: 233419. https://doi.org/10.1016/j.jpowsour.2023.233419

[10] Shi YM, Zhang K, Wang HY et al. Reduced graphene oxide wrapped ZnCo layered double hydroxides microsphere as efficient sulfur host in lithium-sulfur batteries. J Alloy Compd. 2023; 968: 172059. https://doi.org/10.1016/j.jallcom.2023.172059

[11] Wang J, Ellsworth MW. Graphene Aerogels. ECS Transactions. 2009; 19: 241-247. https://doi.org/10.1149/1.3119548

[12] Zhao Y, Hu CG, Hu Y et al. A Versatile, ultralight, nitrogen-doped graphene framework. Angew Chem Int Edit. 2012; 51(45): 11371-11375. https://doi.org/10.1002/ange.201206554

[13] Wang Z, Tian M, Yu J et al. Recent advances of 3D compressible carbon assemblies: A review of synthesis, properties and applications in energy and environment. J Environ Chem Eng. 2021; 9(5): 106269. https://doi.org/10.1016/j.jece.2021.106269

[14] Chen L, Liu S, Guo X, et al. Ultralight, superhydrophobic and fire-resistant nitrogen-doped graphene aerogel for oil/water separation. Separation and Purification Technology. 2024; 330: 125192. https://doi.org/10.1016/j.seppur.2023.125192

[15] Kim MY, Lee JW, Park DJ et al. Highly stable potentiometric sensor with reduced graphene oxide aerogel as a solid contact for detection of nitrate and calcium ions. Electroanal Chem. 2021; 897: 115553. https://doi.org/10.1016/j.jelechem.2021.115553

[16] Cao L, Wang C, Huang Y. Structure optimization of graphene aerogel-based composites and applications in batteries and supercapacitors. Chemical Engineering Journal. 2023; 454: 140094. https://doi.org/10.1016/j.cej.2022.140094

[17] Wu WQ, Du M, Shi HK et al. Application of graphene aerogels in oil spill recovery: A review. Sci Total Environ. 2023; 856: 159107. https://doi.org/10.1016/j.scitotenv.2022.159107

[18] Fan YM, Song WL, Li X, et al. Assembly of graphene aerogels into the 3D biomass-derived carbon frameworks on conductive substrates for flexible supercapacitor. Carbon. 2017; 111: 658-666. https://doi.org/10.1016/j.carbon.2016.10.056

[19] Zhang XY, Zhou J, Zheng YD et al. Graphene-based hybrid aerogels for energy and environmental applications. Chem Eng J. 2021; 420: 129700. https://doi.org/10.1016/j.cej.2021.129700

[20] Wu HY, Wang ZM, Kumagai A et al. Amphiphilic cellulose nanofiber-interwoven graphene aerogel monolith for dyes and silicon oil removal. Compos Sci Technol. 2019; 171: 190-198. https://doi.org/10.1016/j.compscitech.2018.12.017

[21] Sun CZ, Wang ZG, Chen LY et al. Fabrication of robust and compressive chitin and graphene oxide sponges for removal of microplastics with different functional groups. Chem Eng J. 2020; 393: 124796. https://doi.org/10.1016/j.cej.2020.124796

[22] Ji KD, Gao Y, Zhang LF et al. A tunable amphiphilic Enteromorpha-modified graphene aerogel for oil/water separation. Sci Total Environ. 2021; 763: 142958. https://doi.org/10.1016/j.scitotenv.2020.142958

[23] Yue YY, Wang Y, Li JY et al. High strength and ultralight lignin-mediated fire-resistant aerogel for repeated oil/water separation. Carbon. 2022; 193: 285-297. https://doi.org/0.1016/j.carbon.2022.03.015

[24] Wang Q, Wang SL, Yao K et al. Preparation of magnetic lignin/graphene aerogel and its adsorption properties to oil and organic solvents. Ind Crop Prod. 2022; 187: 115372. https://doi.org/10.1016/j.indcrop.2022.115372

[25] Yao WQ, Mao RW, Gao WW et al. Piezoresistive effect of superelastic graphene aerogel spheres. Carbon. 2020; 158: 418-425. https://doi.org/10.1016/j.carbon.2019.11.005

[26] Zhao XX, Xu WL, Chen S et al. Fabrication of super-elastic graphene aerogels by ambient pressure drying and application to adsorption of oils. Chinese J Chem Eng. 2022; 47: 89-97. https://doi.org/10.1016/j.cjche.2021.09.031

[27] Hummers WS, Offeman RE. Preparation of graphite oxide. J Am Chem Soc. 1958; 80: 1339. https://doi.org/10.1021/ja01539a017

[28] McAllister MJ, Li JL, Adamson DH et al. Single sheet functionalized graphene by oxidation and thermal expansion of graphite. Chem Mater. 2007; 19(18), 4396-4404. https://doi.org/10.1021/cm0630800

[29] Hou S, Wu X, Lv Y, et al. Ultralight, highly elastic and bioinspired capillary-driven graphene aerogels for highly efficient organic pollutants absorption. Applied Surface Science. 2020; 509: 144818. https://doi.org/10.1016/j.apsusc.2019.144818

[30] Branchaud BP. Molecularly imprinted materials. J Am Chem Soc. 2005; 127: 14117-14118. https://doi.org/10.1021/ja041037c

[31] Liu T, Huang M, Li X. Highly compressible anisotropic graphene aerogels fabricated by directional freezing for efficient absorption of organic liquids. Carbon. 2016; 100: 456-464. https://doi.org/10.1016/j.carbon.2016.01.038

[32] Xiao JL, Lv W, Song YH et al. Graphene/nanofiber aerogels: Performance regulation towards multiple applications in dye adsorption and oil/water separation. Chem Eng J. 2018; 338: 202-210. https://doi.org/10.1016/j.cej.2017.12.156

[33] Guo S, Yuan H, Liu F, et al. Silver nanowires interlocked graphene aerogel for ultra-high efficient clearage of oil pollution on water. Sustainable Materials and Technologies. 2021; 29: e00285. https://doi.org/10.1016/j.susmat.2021.e00285

[34] Torres CEI, Quezada TES, Kharissova, OV, et al. Carbon-based aerogels and xerogels: synthesis, properties, oil sorption capacities, and DFT simulations. J Environ Chem Eng. 2021; 9(1): 104886. https://doi.org/10.1016/j.jece.2020.104886

[35] Ma W, Zhang M, Liu Z et al. Fabrication of highly durable and robust superhydrophobic-superoleophilic nanofibrous membranes based on a fluorine-free system for efficient oil/water separation. J Membrane Sci. 2019; 570: 303-313. https://doi.org/10.1016/j.memsci.2018.10.035

[36] Wang L, Cheng J, Kang Q, et al. Cobalt-containing nanoparticles embedded in flexible carbon aerogel for spilled oil cleanup and oxygen reduction reaction. Composites Part B: Engineering. 2019; 174: 107039. https://doi.org/10.1016/j.compositesb.2019.107039

[37] Hoviatdoost A, Naderi M, Ghazitabar A, et al. Fabrication of high-performance ultralight and reusable graphene aerogel/cellulose fibers nanocomposite to remove organic pollutants. Materials Today Communications. 2023; 34: 105077. https://doi.org/10.1016/j.mtcomm.2022.105077

[38] Tao Y, Kong D, Zhang C et al. Monolithic carbons with spheroidal and hierarchical pores produced by the linkage of functionalized graphene sheets. Carbon. 2014; 69: 169-177. https://doi.org/10.1016/j.carbon.2013.12.003